

1 ***Listeria monocytogenes* exploits the MICOS complex subunit Mic10 to promote mitochondrial**
2 **fragmentation and cellular infection**

3 Filipe Carvalho^{a,b,c}, Anna Spier^{a,b,c,d,*}, Thibault Chaze^{e,f}, Mariette Matondo^{e,f}, Pascale Cossart^{a,b,c,#},
4 Fabrizia Stavru^{a,b,c,g,*#}

5
6 ^a Unité des Interactions Bactéries-Cellules, Institut Pasteur, Paris, France

7 ^b Institut National de la Santé et de la Recherche Médicale (INSERM), U604, Paris, France

8 ^c Institut National de la Recherche Agronomique (INRA), USC2020, Paris, France

9 ^d Université Paris Diderot, Sorbonne Paris Cité, Paris, France

10 ^e Plateforme Protéomique, Unité de Spectrométrie de Masse pour Biologie (UTechS MSBio), Institut
11 Pasteur, Paris, France

12 ^f Centre National de la Recherche Scientifique (CNRS), USR 2000, Paris, France

13 ^g CNRS, SNC5101, Paris, France

14

15 Running title: *L. monocytogenes* targets Mic10 to fission mitochondria

16 * Present address: Unité de Biologie Evolutive de la Cellule Microbienne, Institut Pasteur, Paris,
17 France

18 # Address correspondence to Pascale Cossart, pascale.cossart@pasteur.fr, or Fabrizia Stavru,
19 fabrizia.stavru@pasteur.fr

20

21 Abstract: 172 words; Text: 4847 words

22

23 **Abstract**

24 Mitochondrial function adapts to cellular demands and is affected by the ability of the organelle to
25 undergo fusion and fission in response to physiological and non-physiological cues. We previously
26 showed that infection with the human bacterial pathogen *Listeria monocytogenes* elicits transient
27 mitochondrial fission and a drop in mitochondrial-dependent energy production through a
28 mechanism requiring the bacterial pore-forming toxin listeriolysin O (LLO). Here, we performed
29 quantitative mitochondrial proteomics to search for host factors involved in *L. monocytogenes*-
30 induced mitochondrial fission. We found that Mic10, a critical component of the mitochondrial
31 contact site and cristae organizing system (MICOS) complex, is significantly enriched in
32 mitochondria isolated from cells infected with wild-type but not with LLO-deficient
33 *L. monocytogenes*. Increased mitochondrial Mic10 levels did not correlate with upregulated
34 transcription, suggesting a post-transcriptional regulation. We showed that Mic10 is necessary for
35 *L. monocytogenes*-induced mitochondrial network fragmentation, and that it contributes to
36 *L. monocytogenes* cellular infection independently of MICOS proteins Mic13, Mic26 and Mic27.
37 Together, *L. monocytogenes* infection allowed us to uncover a role for Mic10 in mitochondrial
38 fission.

39 **Importance.** Pathogenic bacteria can target host cell organelles to take control of key cellular
40 processes and promote their intracellular survival, growth, and persistence. Mitochondria are
41 essential, highly dynamic organelles with pivotal roles in a wide variety of cell functions.
42 Mitochondrial dynamics and function are intimately linked. Our previous research showed that
43 *Listeria monocytogenes* infection impairs mitochondrial function and triggers fission of the
44 mitochondrial network at an early infection stage, in a process that is independent of the main
45 mitochondrial fission protein Drp1. Here, we analyzed how mitochondrial proteins change in
46 response to *L. monocytogenes* infection and found that infection raises the levels of Mic10, a
47 mitochondrial inner membrane protein involved in formation of cristae. We show that Mic10 is

48 important for *L. monocytogenes*-dependent mitochondrial fission and infection of host cells. Our
49 findings thus offer new insight into the mechanisms used by *L. monocytogenes* to hijack
50 mitochondria to optimize host infection.

51 **Introduction**

52 Mitochondria constitute one of the most important eukaryotic organelles due to their role in several
53 essential cellular processes, such as energy production, biosynthesis of metabolic intermediates,
54 calcium storage and signaling, autophagy, apoptosis, as well as redox and innate immune signaling
55 (1–3). The overall morphology and cellular distribution of the mitochondrial network are controlled
56 by a succession of fusion and fission events referred to as “mitochondrial dynamics”. This dynamic
57 equilibrium is fundamental to meet cellular energetic and metabolic demands and respond to stress-
58 inducing conditions (4).

59 Mitochondrial dynamics are governed by a family of large GTPases with membrane-shaping
60 properties necessary to drive fusion or fission of mitochondria (5, 6). Mitochondrial fusion requires
61 the sequential merging of the outer (OMM) and inner mitochondrial membranes (IMM) by the action
62 of the OMM-anchored mitofusin 1 (Mfn1) and 2 (Mfn2) proteins, and the IMM-bound optic atrophy
63 1 (Opa1) protein. Mitochondrial fission is mainly mediated by the cytosolic dynamin-related
64 protein 1 (Drp1), although the endoplasmic reticulum, actin and septins also play significant roles (6,
65 7). The importance of mitochondrial dynamics in cell physiology is attested by numerous neuro-
66 muscular pathologies associated with genetic defects affecting the expression or activity of proteins
67 involved in mitochondrial fusion and fission (8).

68 Due to their involvement in essential cellular processes, mitochondria are an attractive target for viral
69 and bacterial pathogens (9–12). Indeed, many pathogenic bacteria were shown to modulate
70 mitochondrial dynamics to create the ideal conditions for intracellular replication, immune evasion
71 and persistence (11, 13–17). We previously explored how mitochondrial function and dynamics are
72 impacted by infection with *Listeria monocytogenes* (16, 18), a facultative intracellular bacterial
73 pathogen responsible for listeriosis, a life-threatening disease in immunocompromised individuals
74 (19). We showed that *L. monocytogenes* causes fragmentation of the host mitochondrial network
75 early in infection. This event requires the bacterial pore-forming toxin listeriolysin O (LLO), which

76 promotes calcium influx into the host cell (16), causing a drop of the mitochondrial membrane
77 potential and Drp1-independent mitochondrial fission (18). *L. monocytogenes* infection has thus
78 revealed an unconventional mechanism of mitochondrial fission, but the mechanistic details and
79 molecular players involved in modulation of mitochondrial dynamics and function upon
80 *L. monocytogenes* infection still remain unclear.

81 Here, we set out to increase our understanding of the impact of *L. monocytogenes* infection on host
82 cell mitochondria and identify novel factors involved in *L. monocytogenes*-induced mitochondrial
83 fission by performing a quantitative characterization of the mitochondrial proteome upon infection.
84 We report that *L. monocytogenes* infection significantly upregulates the mitochondrial levels of
85 Mic10, a core subunit of the mitochondrial contact site and cristae organizing system (MICOS)
86 complex (20). We show that this increase in Mic10 abundance requires LLO but is not correlated
87 with increased transcription. Finally, we demonstrate that Mic10 is necessary for *L. monocytogenes*-
88 induced mitochondrial fragmentation, and contributes to bacterial infection.

89 **Results**

90 **Quantitative proteomic analysis of the human mitochondrial response to *L. monocytogenes***
91 **infection.** To understand how the human mitochondrial proteome is affected by *L. monocytogenes*
92 infection, we performed quantitative, label-free proteomic analysis of mitochondria isolated from
93 human cells infected with *L. monocytogenes* (Figure 1A). We used HCT116 cells, a human intestinal
94 epithelial cell line rich in mitochondria and efficiently infected by *L. monocytogenes*. Since
95 *L. monocytogenes*-induced mitochondrial fission occurs early in infection and requires LLO (16), we
96 performed short infections (2 h) with wild-type *L. monocytogenes* or with an LLO-deficient strain to
97 focus on LLO-dependent processes. Mitochondria were isolated from infected and uninfected cell
98 lysates by magnetic immunoaffinity purification and mitochondria-associated proteins were
99 processed for LC-MS/MS analysis (Figure 1A). A total of 2,370 unique proteins were identified,
100 with 2,039 (86%) proteins detected in every condition (Figure 1B). Among all identified proteins,
101 862 (36.4%) were annotated as mitochondrial (Figure 1B), which represents a good mitochondrial
102 enrichment degree in our samples (compared to 7–8% of mitochondrial proteins in the human
103 proteome) and a high coverage of the annotated mitochondrial proteome (53% of 1626 proteins;
104 IMPI version Q2, June 2018). This overrepresentation of mitochondrial proteins is reflected in the
105 results of a Gene Ontology (GO) term enrichment analysis, showing eight mitochondrial terms
106 among the ten most enriched GO biological processes (Figure 1C).

107 To determine proteins displaying significantly altered levels with infection, we performed a
108 statistical test on all identified proteins to select those whose abundance changed at least two-fold.
109 We obtained a list of 167 proteins, of which 32 (19.1%) were detected in every condition
110 (Figure 1D). To find proteins that could play a role in mitochondrial fission, we focused on *bona fide*
111 mitochondrial proteins or predicted to be functionally associated and/or interact with mitochondria.
112 According to the IMPI, 35 of the 167 differentially abundant proteins (21%) were annotated as
113 mitochondrial (Figure 1D, Table S1). Among these are proteins involved in the mitochondrial

114 electron transport chain, such as the NADH:ubiquinone oxidoreductase subunit B2 (NDUFB2) and
115 assembly factor DMAC2, the ubiquinol-cytochrome c reductase assembly factors 1 and 3 (UQCC1
116 and UQCC3), the cytochrome c oxidase subunits 6C and 7B (COX6C and COX7B), and the
117 F₁F₀ ATP synthase subunit 6.8PL (ATP5MPL). Four of these proteins become significantly more
118 abundant in response to infection, suggesting an increased activity of the respiratory chain. Other
119 differentially abundant proteins identified in our analysis are associated with mitochondrial
120 translation (cysteinyl- and methionyl-tRNA synthetases 2, CARS2 and MARS2; tRNA
121 isopentenyltransferase 1, TRIT1; and mitochondrial ribosomal proteins CHCHD1 and MRPL42),
122 metabolism of sterols (lanosterol synthase, LSS), fatty acids (hydroxyacyl-thioester dehydratase
123 type 2, HTD2) and branched-chain amino acids (branched-chain ketoacid dehydrogenase kinase,
124 BCKDK), regulation of mitophagy (Bcl2-associated athanogene 5, BAG5 (21, 22); FUN14 domain-
125 containing 1, FUNDC1 (23); peroxiredoxin 6, PRDX6 (24)) and apoptosis (Bcl2-like protein 1,
126 BCL2L1), cristae formation (MICOS complex subunit Mic10, MICOS10), and organelle transport
127 (myosin 19, MYO19 (25)). GO enrichment analysis of the 35 differentially abundant mitochondrial
128 proteins did not reveal any statistically significant overrepresented functional pathways. The
129 mitochondrial abundance of 14 of the 35 proteins (40%) was significantly increased upon infection
130 with wild-type *L. monocytogenes*, whereas it decreased for 8 proteins (23%) (Table S1).
131 Interestingly, 7 of the 14 upregulated proteins and 4 of the 8 downregulated proteins did not display
132 these changes upon infection with LLO-deficient bacteria (Table S1), indicating that LLO triggers
133 such alterations in their mitochondrial abundance.

134 We further focused our attention on proteins predicted to participate in mitochondrial dynamics or
135 membrane-remodeling processes. Interestingly, we found Mic10 among the seven proteins enriched
136 in mitochondria in response to infection by wild-type but not LLO-deficient *L. monocytogenes*
137 (Figure 1E). Mic10 is a core subunit of the mitochondrial contact site and cristae organizing system
138 (MICOS) complex, a conserved IMM complex responsible for the formation of crista junctions (sites

139 where the IMM invaginates to form cristae) (20). Importantly, Mic10 is a small transmembrane
140 protein, whose V-shaped membrane topology and ability to oligomerize provide it with membrane-
141 bending properties that are fundamental for driving the formation of crista junctions (26, 27).

142

143 **Mic10 is required for *L. monocytogenes*-induced mitochondrial network fragmentation.** To
144 investigate the role of Mic10 in *L. monocytogenes* infection-induced mitochondrial fission, we either
145 lowered or raised Mic10 levels in host cells before infection and analyzed how the mitochondrial
146 network morphology was affected. To assess the effect of Mic10 depletion, we used U2OS cells
147 because its mitochondrial morphology is better suited for microscopy analysis compared to HCT116
148 cells. U2OS were transfected with non-targeting control (si-Ctrl) or Mic10-targeting (si-Mic10)
149 siRNAs (Figure 2A), after which they were left uninfected or infected with wild-type or LLO-
150 deficient bacteria. Cells were fixed and mitochondria immunolabeled for confocal microscopy
151 analysis. In agreement with our previous results, si-Ctrl cells showed a typical tubular mitochondrial
152 network, which became fragmented upon infection with wild-type, but not LLO-deficient bacteria
153 (Figure 2B). In si-Mic10 cells, the mitochondrial morphology was similar to that of si-Ctrl cells,
154 indicating that Mic10 knockdown does not affect mitochondrial network shape. However, unlike si-
155 Ctrl cells, mitochondrial fragmentation was not detected in si-Mic10 cells in response to wild-type
156 *L. monocytogenes* (Figure 2B). To obtain an unbiased, quantitative representation of these
157 observations, we used a semi-automated morphometric tool to analyze the mitochondrial network
158 morphology from a large number of cells, which allowed us to calculate a mitochondrial
159 fragmentation degree per cell. Results confirmed that the mitochondrial network of si-Mic10 cells
160 does not undergo fragmentation in the presence of *L. monocytogenes*, in contrast to si-Ctrl cells
161 (Figure 2C). We also performed this experiment in HCT116 cells and obtained similar results
162 (Figure S1), thus corroborating the crucial role of Mic10 in mediating mitochondrial fission in
163 response to *L. monocytogenes* infection.

164 Next, we examined the effect of increased Mic10 levels in *Listeria*-dependent mitochondrial fission.
165 We followed the experimental approach described earlier but instead of siRNA, cells were
166 transfected with a plasmid driving the constitutive expression of a C-terminal FLAG fusion of the
167 human Mic10 protein (Mic10-FLAG), or the empty parental plasmid as a control. We observed that
168 constitutive expression of Mic10-FLAG resulted in a concomitant reduction of the endogenous
169 Mic10 levels (Figure 3A). This effect was previously reported for both Mic10 and Mic60 and
170 suggests a tight regulation of the total levels of MICOS proteins (28). Whereas control plasmid-
171 transfected cells displayed a fragmented mitochondrial network upon infection with wild-type but
172 not LLO-deficient bacteria (Figure 3B,C), cells expressing high levels of exogenous Mic10-FLAG
173 showed a highly vesiculated mitochondrial network, even in the absence of infection (Figure 3B,C).
174 Unlike Mic10 depletion, which does not affect the mitochondrial network morphology
175 (Figures 2B,C), excessive mitochondrial levels of Mic10 cause a collapse of the mitochondrial
176 network.

177 These results indicate that *L. monocytogenes* requires basal Mic10 levels to trigger mitochondrial
178 fission in an LLO-dependent manner. Moreover, together with our proteomic data, they suggest that
179 this mitochondrial network breakdown could be a result of increased Mic10 levels in mitochondria.

180

181 **Mic10 contributes to an efficient *L. monocytogenes* cellular infection.** The dynamic state of the
182 mitochondrial network was reported to play a role in the early steps of *L. monocytogenes* cellular
183 infection, as cells with fragmented mitochondria were less susceptible to infection, whereas cells
184 with hyperfused mitochondria showed improved infection levels (16). Considering our results
185 regarding the effect of Mic10 levels on the morphological status of the mitochondrial network, we
186 wondered whether and how Mic10 levels affect *L. monocytogenes* infection. We performed
187 gentamicin protection assays in control cells and in cells either depleted of Mic10 or overexpressing
188 Mic10, and after infection with wild-type bacteria, we quantified the intracellular bacterial load.

189 Compared to control cells, Mic10-depleted cells were 30% less infected (Figure 4A), whereas cells
190 overexpressing Mic10 showed a 20% increase in infection (Figure 4B). To determine if the reduced
191 infection levels observed under Mic10 depletion were due to alterations in cellular bioenergetics
192 elicited by defects in mitochondrial function and energy metabolism, we analyzed the mitochondrial
193 respiratory and ATP production capacity of these cells. The oxygen consumption rate and ATP
194 levels in si-Mic10 cells were similar to those in si-Ctrl cells (Figure 4C,D), in agreement with other
195 studies (29, 30). These results suggest that the effect of Mic10 on *L. monocytogenes* infection is not
196 caused by changes in mitochondrial energy production.

197 Depletion of Mic10 in yeast and mammalian cells results in reduced levels of MICOS proteins
198 Mic13, Mic26 and Mic27 (26, 28, 31, 32), which interact closely with Mic10 to form the Mic10
199 subcomplex (20). We thus assessed if the decreased *Listeria* infection associated with Mic10
200 knockdown was a consequence of the lower abundance of Mic13, Mic26 and/or Mic27 by
201 performing siRNA-mediated silencing of the corresponding genes before infection with wild-type
202 *L. monocytogenes*. We confirmed that Mic10 depletion results in partial downregulation of the other
203 three members of the Mic10 subcomplex (Figure 4E). In turn, Mic13 and, to a lesser degree, Mic27,
204 are also necessary to sustain basal Mic10 levels (Figure 4E), in agreement with previous reports (31,
205 32). Quantification of intracellular bacteria showed again impaired infection of Mic10-depleted cells,
206 but revealed no difference between control cells and cells depleted for either Mic13, Mic26 or Mic27
207 (Figure 4F). This surprising result demonstrates that none of these MICOS subunits is individually
208 required for *Listeria* cellular infection, and therefore supports a unique role of Mic10 in this process.
209 In agreement with this finding, besides Mic10, none of the other six subunits of the metazoan
210 MICOS complex (Mic13, Mic19, Mic25, Mic26, Mic27, and Mic60) showed significantly changed
211 levels with *L. monocytogenes* infection in our proteomic analysis. We investigated if increased
212 Mic10 levels resulted from infection-driven transcriptional upregulation. Quantitative real-time PCR
213 analysis of RNAs from cells infected or not with wild-type bacteria showed that the relative level of

214 transcripts coding for Mic10 or any other MICOS subunits remained unchanged upon
215 *L. monocytogenes* infection (Figure S2). This result suggests that instead of upregulating Mic10
216 transcription to elevate its protein levels, *L. monocytogenes* infection promotes an accumulation of
217 Mic10 in mitochondria through an unknown post-transcriptional mechanism.

218 Overall, these results indicate that *Listeria* cellular infection efficiency is specifically and positively
219 correlated with increased mitochondrial levels of Mic10.

220 **Discussion**

221 Bacterial pathogens like *L. monocytogenes*, *Legionella pneumophila*, *Shigella flexneri*, *Chlamydia*
222 *trachomatis* and *Mycobacterium tuberculosis* interfere with mitochondrial dynamics to create an
223 intracellular environment suited for survival and persistence (14–16, 18, 33–35). In particular,
224 *L. monocytogenes* was shown to induce mitochondrial fission early in infection and cause a
225 metabolic slowdown (16, 18), delaying mitochondria-dependent cellular responses, such as type III
226 interferon signaling (36). Here, we employed quantitative proteomics to characterize the
227 mitochondrial response to *L. monocytogenes* infection and search for host factors involved in
228 *L. monocytogenes*-induced mitochondrial fission. We revealed the MICOS complex protein Mic10
229 as a new player in this process. We showed that *L. monocytogenes* infection increases Mic10 levels
230 in mitochondria in an LLO-dependent manner, and that Mic10 abundance is positively correlated
231 with *L. monocytogenes*-induced mitochondrial fragmentation and host cell infection. This supports a
232 model whereby *L. monocytogenes* infection promotes elevated mitochondrial Mic10 levels to trigger
233 organellar fission and favor cellular infection.

234 Our proteomic approach yielded a degree of mitochondrial enrichment (36%) and mitochondrial
235 proteome coverage (53%) comparable to those reported in other studies using varied mitochondrial
236 isolation and mass spectrometry protocols (37–39). One of these studies explored the host
237 mitochondrial response to *M. tuberculosis* infection, showing that virulent strains increased
238 mitochondrial energy production and protected host cells from apoptosis, as opposed to avirulent
239 bacteria (37). These changes were partially supported at the protein level, with upregulation of
240 proteins involved in respiration and anti-apoptotic mechanisms, and reduced levels of proteins linked
241 to anti-microbial response. Our proteomic data also hint that mitochondrial translation and
242 respiration are enhanced in response to *L. monocytogenes* infection, possibly to compensate for the
243 drop in mitochondrial membrane potential (16).

244 We chose to explore Mic10 because it represents a *bona fide* IMM protein with well-characterized
245 membrane-shaping properties (26, 27, 40–42), and its mitochondrial levels showed an LLO-
246 dependent upsurge with infection. We hypothesized that elevated Mic10 levels could drive
247 deregulated IMM remodeling, resulting in mitochondrial fission. In support of this assumption, we
248 showed that *L. monocytogenes* cannot fragment mitochondria in Mic10-depleted cells. In contrast,
249 we observed clear mitochondrial fragmentation in cells overexpressing Mic10, even in the absence
250 of bacteria. Others have reported that excessive Mic10 levels disrupt cristae structure (26), and that
251 Mic10 knockdown or knockout also result in absent cristae junctions and unattached cristae stacked
252 in the matrix (26–30, 40, 43). These phenotypes showcase the importance of Mic10 in IMM
253 structure maintenance and suggest that *L. monocytogenes* could target Mic10 to induce IMM
254 remodeling and trigger mitochondrial fission. We did not observe changes in the mitochondrial
255 morphology of Mic10-depleted cells, implying that the ultrastructural defects caused by Mic10
256 knockdown are not sufficient to elicit mitochondrial fragmentation, in contrast to the disruptive
257 effect of excessive Mic10 levels. Consistently, knockdown of other MICOS subunits, such as Mic60
258 (28), Mic19 and Mic25 (44), did not cause mitochondrial fragmentation, although Mic60- and
259 Mic19-depleted mitochondria showed bulb-like enlargements (28, 44). Similar features were
260 reported in Mic10-null yeast mitochondria (45), but we did not observe them in our si-Mic10 cells.
261 Surprisingly, the enrichment of Mic10 in mitochondria upon *L. monocytogenes* infection was not due
262 to increased Mic10 transcription, which suggests that Mic10 accumulation in mitochondria occurs at
263 the protein level. This could be caused by increased import or reduced turnover of Mic10 in
264 mitochondria. As a nuclear gene-encoded protein, Mic10 is imported from the cytosol via the
265 mitochondrial protein import machinery (46, 47). However, as other MICOS proteins are similarly
266 imported (47), and our proteomics data showed no significant changes in their mitochondrial levels,
267 it seems unlikely that increased Mic10 levels are caused by enhanced mitochondria import. Protein
268 turnover in mitochondria is carried out by multiple proteases residing in the different mitochondrial

269 compartments (48). Interestingly, two of these proteases, Yme1L and Oma1, were reported to
270 participate in the processing of Mic60 and Mic19, respectively (28, 44), suggesting that they may
271 participate in Mic10 proteolysis. Future knockdown or loss-of-function experiments should clarify
272 the involvement of Yme1L and/or Oma1 in Mic10 turnover.

273 Cells with fragmented mitochondria were shown to be less infected by *L. monocytogenes*, raising the
274 hypothesis that pre-fragmented mitochondria are more resistant to the *L. monocytogenes*-induced
275 bioenergetic slowdown (16). Here, we demonstrate that *L. monocytogenes* infection is partially
276 impaired in cells with reduced Mic10 abundance, suggesting that Mic10-dependent mitochondrial
277 fission induced by *L. monocytogenes* is important for subsequent cellular infection. In contrast,
278 bacterial infection was improved by 20% in cells transfected with DNA driving Mic10
279 overexpression. Since not every cell overexpressed Mic10, it is possible that this margin may be
280 higher. Further experiments using stable clones of Mic10-overexpressing cells will be helpful to
281 confirm whether *Listeria* infection is enhanced due to increased mitochondrial Mic10 levels.

282 An important question is how *L. monocytogenes* manipulates events taking place inside
283 mitochondria, even at early steps of infection when it is entering host cells or possibly still in the
284 extracellular medium. The obvious trigger is LLO secreted by *L. monocytogenes*, which mediates
285 Ca^{2+} influx into the host cytoplasm (16, 49, 50). Mitochondria take up Ca^{2+} from the cytosol via the
286 mitochondrial calcium uniporter (MCU) complex (3), which includes the mitochondrial calcium
287 uptake protein 1 (MICU1) that controls the Ca^{2+} concentration crossing the MCU channel (51).
288 Interestingly, MICU1 was identified in our proteomic analysis, showing an apparent enrichment with
289 *L. monocytogenes* infection in an LLO-dependent manner (Table S1). Mitochondrial Ca^{2+} efflux is
290 mediated, among others, by the sodium/calcium exchanger NCLX (52), which can be activated by
291 protein kinase A (PKA)-mediated phosphorylation (53). The catalytic subunit alpha of PKA
292 (PRKACA) is one of four mitochondria-related proteins that are less abundant with infection in an
293 LLO-dependent manner, suggesting that PKA-mediated NCLX activation is impaired during

294 *L. monocytogenes* infection. MICU1 upregulation and NCLX inhibition could result in increased
295 mitochondrial Ca^{2+} concentration and, among other effects, a generalized collapse of the
296 mitochondrial network (54). An investigation on the contribution of these mitochondrial proteins
297 could clarify a role for mitochondrial Ca^{2+} uptake in *L. monocytogenes*- and possibly also Mic10-
298 dependent mitochondrial fragmentation.

299 In conclusion, this work represents the first proteomic analysis of the mitochondrial response to
300 *L. monocytogenes* infection and allowed us to reveal a novel actor in mitochondrial dynamics, which
301 is specifically manipulated by *L. monocytogenes* to create the ideal setting for host cell infection.

302

303 **Materials and methods**

304 **Bacterial strains, cell lines and growth conditions.** The following *Listeria monocytogenes* strains
305 were used in this study: wild type EGD (BUG 600), its isogenic LLO mutant EGD Δ *hly* (BUG 3650),
306 and the corresponding GFP-expressing derivatives EGD-cGFP (BUG 2539) and EGD Δ *hly*-cGFP
307 (BUG 2786). Bacteria were grown at 37 °C in brain heart infusion (BHI) media (Difco, BD),
308 supplemented with chloramphenicol (7 µg/mL), when required. The following tissue culture cell
309 lines were used in this study: HCT116 (human colorectal adenocarcinoma; ATCC CCL-247) and
310 U2OS (human osteosarcoma; ATCC HTB-96). Cells were maintained in McCoy's 5A GlutaMAX
311 medium (Gibco), supplemented with 1 mM non-essential amino acids (Gibco) and 10% (v/v) fetal
312 bovine serum (FBS) (BioWest), and grown at 37 °C in a humidified 10% CO₂ atmosphere.

313

314 **Cell transfection.** For transient gene knockdown, cells were reverse transfected with siRNAs in 24-
315 well plates, using Lipofectamine RNAiMax (Invitrogen) according to the manufacturer's
316 instructions, except that McCoy's 5A was used as dilution medium. The medium was changed the
317 following day and cells were assayed 48 h post-transfection. siRNA duplexes were used at the
318 following concentrations: siRNA Universal Negative Control #1 (Sigma-Aldrich) and Mic10 (5'-
319 CGGAUGCGGUCGUGAAGAAtt-3'; Eurofins Genomics) at 100 nM; Mic13 (Ambion, Silencer
320 Select #s195661), Mic26 (Ambion, Silencer Select #s35601), and Mic27 (Ambion, Silencer Select
321 #s225655) at 20 nM. For transient overexpression of Mic10, cells were seeded in 24-well plates one
322 day before transfection with 0.5 µg of Mic10-FLAG plasmid DNA (pcDNA3.1(+)-MINOS1-DYK;
323 GenScript, ORF cDNA clone ID OHu15514), using jetPRIME (Polyplus Transfection) according to
324 the manufacturer's instructions. Control cells were transfected with empty plasmid DNA
325 (pcDNA3.1(+); Invitrogen). Cells were assayed 24 h post-transfection. For immunofluorescence,
326 cells were seeded in wells containing glass coverslips.

327

328 **Cell infections.** For cell infection assays, confluent monolayers were incubated for 1 h at 37 °C in
329 FBS-free cell culture medium alone (non-infected cells) or inoculated with logarithmic phase
330 bacteria (OD_{600nm} 0.6–1.0) at a multiplicity of infection (MOI, bacteria/cell) of 20 (for HCT116
331 cells) or 50 (for U2OS cells). Medium was removed and cells were incubated for another hour (total
332 infection time: 2 h) at 37 °C in FBS-containing culture medium supplemented with 20 µg/mL
333 gentamicin sulfate (Sigma-Aldrich), to kill extracellular bacteria. Cells were then washed with
334 Dulbecco's phosphate-buffered saline (DPBS; Gibco) before processing for further analyses. For
335 immunofluorescence, cells were infected with GFP-expressing *L. monocytogenes* strains. To
336 quantify intracellular bacterial levels, infected cells were lysed in ice-cold 0.2% (v/v) Triton X-100
337 in DPBS, serially diluted in DPBS, and plated on BHI agar plates. Colony-forming units (CFUs)
338 were counted after 24 h of incubation at 37 °C and bacterial numbers were normalized to the
339 inoculum concentration.

340

341 **Mitochondrial isolation and LC-MS/MS sample preparation.** For label-free quantitative
342 proteomic analysis of mitochondria, HCT116 cells (~5×10⁷) cultivated in 150-mm dishes were
343 treated as outlined in Figure 1A. Cells were left uninfected (NI) or infected either with wild type (*Lm*
344 WT) or LLO-deficient EGD (*Lm* Δ*hly*), as described above. Three independent biological replicates
345 were prepared and analyzed for each condition. After infection, mitochondria were isolated from
346 cells by magnetic immunoaffinity separation, using the Mitochondria Isolation Kit (human; Miltenyi
347 Biotec). For this, cells were washed with ice-cold DPBS and scraped in ice-cold kit lysis buffer
348 (1 mL/10⁷ cells) containing a cocktail of protease inhibitors (cOmplete, EDTA-free; Roche). Cells
349 were then lysed in a Potter-Elvehjem homogenizer (~50 strokes), with lysis monitored by trypan blue
350 staining. Lysates were centrifuged for 5 min at 800×g (4 °C) to pellet unbroken cells, and the
351 supernatant was recovered for magnetic labeling and separation of mitochondria as detailed in the kit

352 instructions. Purified mitochondria were resuspended in urea lysis buffer (20 mM HEPES pH 8.0,
353 8 M urea) and protein concentration was measured with BCA Protein Assay kit (Pierce). Proteins
354 were reduced for 30 min at 55 °C in the presence of 25 mM DTT, and then alkylated for 15 min in
355 the dark in the presence of 50 mM iodoacetamide. Samples were diluted two-fold with 20 mM
356 HEPES pH 8.0 and proteins digested with Lys-C (Promega) at a protease/protein ratio of 1:100
357 (w/w) for 4 h at 37 °C. Samples were diluted two-fold again and incubated overnight at 37 °C with
358 trypsin (sequencing grade modified, Promega) at a 1:50 (w/w) ratio. Formic acid (FA) was added at
359 1% (v/v), and after 10 min on ice, samples were centrifuged for 10 min at 10,000×g to pellet any
360 insoluble material. Peptides in the supernatant were purified in Sep-Pak C18 cartridges (100 mg;
361 Waters), lyophilized, dissolved in solvent A [0.1% (v/v) FA in water/acetonitrile (ACN) (98:2, v/v)]
362 and quantified by absorbance at 280 nm (NanoDrop, Thermo Fisher Scientific). Samples were
363 analyzed by LC-MS/MS as described in Text S1.

364

365 **Immunofluorescence.** Cells grown on glass coverslips were fixed for 15 min at room temperature in
366 4% (v/v) paraformaldehyde in PBS, permeabilized for 5 min in 0.5% (v/v) Triton X-100 in PBS, and
367 blocked for 20 min in blocking buffer [1% (w/v) BSA, 10% (v/v) goat serum in PBS]. Labelling with
368 primary and fluorophore-conjugated secondary antibodies or dyes was performed in blocking buffer
369 for 1 h at room temperature. Cells were washed three times in PBS between every step after fixation,
370 except after blocking. Coverslips were mounted onto microscope slides with FluoroMount-G
371 mounting medium (Interchim), and imaged the next day or stored in the dark at 4 °C. Primary
372 antibodies were used as follows: rabbit polyclonal anti-C1ORF151/Mic10 (1:200; Abcam, ab84969),
373 mouse monoclonal anti-Tom20 clone 29 (1:200; BD Transduction Laboratories), rabbit polyclonal
374 anti-Tom20 clone F-10 (1:200; Santa Cruz Biotechnology), and mouse monoclonal anti-FLAG clone
375 M2 (1:100; Sigma-Aldrich). Anti-rabbit and anti-mouse antibodies conjugated to Alexa Fluor 568
376 and 647 dyes (1:500; Molecular Probes) were used as secondary antibodies; Hoescht 33342

377 (Molecular Probes) was used to stain DNA. Cells were analyzed in a ZEISS AxioObserver.Z1
378 inverted microscope (Carl Zeiss AG) equipped with a high-speed CSU-X1 spinning-disk confocal
379 system (Yokogawa) and an Evolve EM-CCD camera (Photometrics). Single focal plane images were
380 acquired through a Plan-Apochromat 63×/1.4 Ph3 oil objective across multiple wavelength channels,
381 using MetaMorph software (version 7.7.9.0). Fiji was used for image processing, including channel
382 color selection, brightness and contrast adjustment, addition of scale bars and generation of
383 composite images.

384

385 **Mitochondrial morphology analysis.** Confocal images of cells were taken from various fields of
386 view randomly selected across the entire coverslip area and their mitochondrial morphology was
387 analyzed using the semi-automated morphometric tool MiNA within Fiji (55). Mitochondrial
388 networks (labeled with anti-Tom20) from individual cells were selected and digitally isolated before
389 batch analysis. From the output data, a ratio of the values listed under the “Individuals” (number of
390 unbranched mitochondrial particles, e.g. puncta and rods) and “Mitochondrial footprint”
391 (mitochondrial area) parameters was calculated to determine the degree of mitochondrial
392 fragmentation per analyzed cell. A minimum of 50 cells were analyzed per condition, in a total of
393 three independent experiments.

394

395 **Statistics.** Statistical analyses were performed in Prism 8 (GraphPad Software). Unpaired two-tailed
396 Student’s t-test was used to compare the means of two groups; one-way ANOVA was used with
397 Tukey’s post-hoc test for pairwise comparison of means from more than two groups, or with
398 Dunnett’s post-hoc test for comparison of means relative to the mean of a control group. Difference
399 between group means were considered statistically significant at p-value < 0.05. Significance levels

400 are indicated as: ns, not significant ($p > 0.05$); *, $p < 0.05$; **, $p < 0.01$; ***, $p < 0.001$, ****,
401 $p < 0.0001$.

402

403 **Data availability.** Mass spectrometry proteomics data have been deposited to the ProteomeXchange

404 Consortium via the PRIDE (56) partner repository with the dataset identifier PXD014667.

405 **Acknowledgements**

406 We thank current and past lab members for helpful discussions; Francis Impens and Evy
407 Timmerman (VIB Proteomics Core, University of Ghent, Belgium) for training and assistance with
408 proteomic analyses; and Alessandro Pagliuso for critical reading of the manuscript.

409 This study was supported by grants to P.C. from the European Research Council (H2020-ERC-2014-
410 ADG 670823-BacCellEpi), the Agence Nationale de la Recherche (ANR) and the French
411 Government's "Investissements d'Avenir" program Laboratoires d'Excellence "Integrative Biology
412 of Emerging Infectious Diseases" (LabEx IBEID, ANR-10-LABX-62-IBEID). A.S. was supported
413 by a BioSPC doctoral fellowship from the Université Paris Diderot. P.C. is a Senior International
414 Research Scholar of the Howard Hughes Medical Institute. F.S. is a CNRS permanent researcher.

415

416 **Figure legends**

417 **Figure 1 – Analysis of changes in the human mitochondrial proteome elicited by**
418 ***L. monocytogenes* infection.**

419 A) Schematic diagram of the experimental procedure used for proteomic analysis of human
420 mitochondria isolated from cells infected or not with *L. monocytogenes*.

421 B) Venn diagram of unique and common proteins identified in mitochondria isolated from
422 uninfected and *L. monocytogenes*-infected cells. Pie chart shows distribution of proteins classified as
423 mitochondrial and non-mitochondrial according to MitoMiner's IMPI database (Q2, 2018).

424 C) Top ten most prevalent Gene Ontology (GO) biological processes obtained from functional
425 enrichment analysis (PANTHER gene analysis tool) of all proteins identified in mitochondria
426 isolated from uninfected and *L. monocytogenes*-infected cells.

427 D) Venn diagram of unique and common proteins identified in mitochondria isolated from
428 uninfected and *L. monocytogenes*-infected cells with statistically significant changes in their
429 abundance (fold change>2, FDR=0.05). Pie chart shows distribution of differentially abundant
430 proteins classified as mitochondrial and non-mitochondrial according to MitoMiner's IMPI database
431 (Q2, 2018).

432 E) Heat map showing relative changes in abundance of the 35 proteins annotated as mitochondrial in
433 D. For each protein, the intensity levels in every condition (each box represents a triplicate) were
434 normalized to the mean value using Z-score. Intensity levels higher and lower than the mean are
435 indicated in green and red shades, respectively. Proteins are indicated by their gene symbol.

436

437 **Figure 2 – Mic10 knockdown blocks *L. monocytogenes*-induced mitochondrial fragmentation.**

438 A) Immunoblot analysis of Mic10 levels in U2OS osteosarcoma cells transfected with control
439 negative (si-Ctrl) or Mic10-targeting (si-Mic10) siRNAs. Beta-actin protein was used as loading
440 control.

441 B) Immunofluorescence analysis of U2OS cells transfected with control negative (si-Ctrl) or Mic10-
442 targeting (si-Mic10) siRNAs, which were left uninfected (NI) or infected (MOI 50, 2h) with GFP-
443 expressing wild type (*Lm* WT) or LLO-deficient (*Lm* Δ hly) *L. monocytogenes*. Mic10 is shown in
444 green, mitochondria (anti-Tom20) in red, nuclei (Hoescht 33342) in blue, and bacteria (*Lm*) in
445 yellow. White box indicates a region of the mitochondrial network magnified (2x) in the inset shown
446 below (mitochondrial labeling only). Scale bar (top right): 10 μ m.

447 C) Quantitative analysis of the mitochondrial fragmentation degree in U2OS cells analyzed in B.
448 Mitochondrial network morphology was analyzed using the morphometric ImageJ plugin tool MiNA
449 on mitochondria-labeled images. Fragmentation degree per analyzed cell was determined by the ratio
450 between number of individual mitochondrial particles and total mitochondrial area. Scatter plot
451 graph shows mitochondrial fragmentation degree values for each analyzed cell (dots, n>95) and the
452 mean (horizontal bar). Statistically significant differences were determined by one-way ANOVA
453 with Tukey's post-hoc test: *** p<0.001; **** p<0.0001.

454

455 **Figure 3 – Mic10 overexpression triggers mitochondrial fragmentation regardless of**
456 ***L. monocytogenes* infection.**

457 A) Immunoblot analysis of Mic10 levels in HCT116 cells transiently transfected with control
458 plasmid (Ctrl) or a plasmid constitutively expressing C-terminal FLAG-tagged Mic10 (Mic10-
459 FLAG). Both endogenous Mic10 and exogenous Mic10-FLAG were detected with an anti-Mic10
460 antibody. Beta-actin protein was used as loading control.

461 B) Immunofluorescence analysis of HCT116 cells transiently transfected with control plasmid (Ctrl)
462 or a plasmid constitutively expressing C-terminal FLAG-tagged Mic10 (Mic10-FLAG), which were
463 left uninfected (NI) or infected (MOI 20, 2h) with GFP-expressing wild type (*Lm* WT) or LLO-
464 deficient (*Lm* Δ hly) *L. monocytogenes*. Mitochondria (anti-Tom20) is shown in red, Mic10-FLAG
465 (anti-FLAG) in green, nuclei (Hoescht 33342) in blue, and bacteria (*Lm*) in yellow. White box
466 indicates a region of the mitochondrial network magnified (2x) in the inset shown below
467 (mitochondrial labeling only). Scale bar (top right): 10 μ m.

468 C) Quantitative analysis of the mitochondrial fragmentation degree in cells analyzed in B.
469 Mitochondrial network morphology was analyzed using the morphometric ImageJ plugin tool MiNA
470 on mitochondria-labeled images. Fragmentation degree per analyzed cell was determined by the ratio
471 between number of individual mitochondrial particles and total mitochondrial area. Scatter plot
472 graph shows mitochondrial fragmentation degree values for each analyzed cell (dots, n>70) and the
473 mean (horizontal bar), and is representative of three independent experiments. Statistically
474 significant differences were determined by one-way ANOVA with Tukey's post-hoc test: ****
475 p<0.0001.

476

477 **Figure 4 – Mic10 contributes to *L. monocytogenes* cellular infection.**

478 A) Quantification of intracellular bacteria in HCT116 cells transfected with control negative (si-Ctrl)
479 or Mic10-targeting (si-Mic10) siRNAs, following infection with wild type *L. monocytogenes* (MOI
480 20, 2h). Results are shown as mean \pm SEM of three independent experiments, and represented as
481 percentage of intracellular bacteria relative to those quantified in si-Ctrl cells. Statistically significant
482 difference was determined by unpaired, two-tailed t-test: *** p<0.001.

483 B) Quantification of intracellular bacteria in HCT116 cells transiently transfected with control
484 plasmid (Ctrl) or a plasmid constitutively expressing C-terminal FLAG-tagged Mic10 (Mic10-

485 FLAG), following infection with wild type *L. monocytogenes* (MOI 20, 2h). Results are expressed as
486 percentage of intracellular bacteria relative to those quantified in Ctrl cells, and shown as mean \pm
487 SEM of three independent experiments. Statistically significant difference was determined by
488 unpaired, two-tailed t-test: *** $p < 0.001$.

489 C) Oxygen consumption rate (OCR, pmol/min) of HCT116 cells transfected with control negative
490 (si-Ctrl) or Mic10-targeting (si-Mic10) siRNAs was measured in a Seahorse XF Analyzer. Electron
491 transport chain inhibitors (oligomycin, FCCP, and antimycin A/rotenone) were added at defined time
492 points to monitor specific components of cellular respiration. Results are expressed as fraction of the
493 first OCR value (basal respiration) of si-Ctrl cells, and shown as mean \pm SEM of three independent
494 experiments.

495 D) Cellular ATP levels in HCT116 cells transfected with control negative (si-Ctrl) or Mic10-
496 targeting (si-Mic10) siRNAs were quantified by luminescence-based plate assay, using ATPlite
497 Luminescence Assay kit. Negative controls consist of cells treated with Triton X-100 (TX100).
498 Results are expressed as percentage of ATP levels relative to those quantified in si-Ctrl cells, and
499 shown as mean \pm SEM of three independent experiments. Statistically significant differences were
500 determined by unpaired, two-tailed t-test: ns, not significant.

501 E) Immunoblot analysis of the levels of Mic10 subcomplex members (Mic10, Mic13, Mic26 and
502 Mic27) in HCT116 cells transfected with control negative siRNA (si-Ctrl), or siRNA targeting
503 Mic10 (si-Mic10), Mic13 (si-Mic13), Mic26 (si-Mic26) or Mic27 (si-Mic27). Beta-actin protein was
504 used as loading control.

505 F) Quantification of intracellular bacteria in cells treated as in E, after infection with wild type
506 *L. monocytogenes* (MOI 20, 2h). Results are shown as mean \pm SEM of three independent
507 experiments, and represented as percentage of intracellular bacteria relative to those quantified in si-

508 Ctrl cells. Statistical significance was determined by one-way ANOVA with Dunnett's post-hoc
509 test: ns, not significant; ** p<0.01.

510

511 **Figure S1 – Confirmation of Mic10-dependent *L. monocytogenes*-induced mitochondrial**
512 **fragmentation in HCT116 cells.**

513 A) Immunoblot analysis of Mic10 levels in HCT116 cells transfected with control negative (si-Ctrl)
514 or Mic10-targeting (si-Mic10) siRNAs. Beta-actin protein was used as loading control.

515 B) Immunofluorescence analysis of HCT116 cells transfected with control negative (si-Ctrl) or
516 Mic10-targeting (si-Mic10) siRNAs, which were left uninfected (NI) or infected (MOI 20, 2h) with
517 GFP-expressing wild type (*Lm* WT) or LLO-deficient (*Lm* Δ hly) *L. monocytogenes*. Mic10 is shown
518 in green, mitochondria (anti-Tom20) in red, nuclei (Hoescht 33342) in blue, and bacteria (*Lm*) in
519 yellow. White box indicates a region of the mitochondrial network magnified (2x) in the inset shown
520 below (mitochondrial labeling only). Scale bar (top right): 10 μ m.

521 C) Quantitative analysis of the mitochondrial fragmentation degree in cells analyzed in B.
522 Mitochondrial network morphology was analyzed using the morphometric ImageJ plugin tool MiNA
523 on mitochondria-labeled images. Fragmentation degree per analyzed cell was determined by the ratio
524 between number of individual mitochondrial particles and total mitochondrial area. Scatter plot
525 graph shows mitochondrial fragmentation degree values for each analyzed cell (dots, n>50) and the
526 mean (horizontal bar), and is representative of three independent experiments. Statistically
527 significant differences were determined by one-way ANOVA with Tukey's post-hoc test: * p<0.05;
528 ** p<0.01, *** p<0.001.

529

530 **Figure S2 – Transcription of Mic10 or any other MICOS complex genes is not upregulated**
531 **upon *L. monocytogenes* infection.**

532 Analysis of gene expression of human MICOS complex subunits Mic10, Mic13, Mic19, Mic25,
533 Mic26, Mic27, and Mic60 in response to *L. monocytogenes* infection. HCT116 cells were left
534 uninfected (NI) or infected (MOI 20, 2h) with wild type (*Lm* WT) or LLO-deficient (*Lm* Δ hly)
535 *L. monocytogenes*, and total cellular RNAs were isolated and used for RT-qPCR analysis. Results are
536 shown as mean \pm SEM of three independent experiments, and represented as fold change in
537 transcript levels relative to those in NI cells.

538

539 **References**

- 540 1. Spinelli JB, Haigis MC. 2018. The multifaceted contributions of mitochondria to cellular
541 metabolism. *Nat Cell Biol* 20:745–754.
- 542 2. Tait SWG, Green DR. 2012. Mitochondria and cell signalling. *J Cell Sci* 125:807–15.
- 543 3. Giorgi C, Marchi S, Pinton P. 2018. The machineries, regulation and cellular functions of
544 mitochondrial calcium. *Nat Rev Mol Cell Biol* 19:713–730.
- 545 4. Wai T, Langer T. 2016. Mitochondrial Dynamics and Metabolic Regulation. *Trends*
546 *Endocrinol Metab* 27:105–17.
- 547 5. Tilokani L, Nagashima S, Paupe V, Prudent J. 2018. Mitochondrial dynamics: overview of
548 molecular mechanisms. *Essays Biochem* 62:341–360.
- 549 6. Pagliuso A, Cossart P, Stavru F. 2017. The ever-growing complexity of the mitochondrial
550 fission machinery. *Cell Mol Life Sci*.
- 551 7. Kraus F, Ryan MT. 2017. The constriction and scission machineries involved in mitochondrial
552 fission. *J Cell Sci* 2;jcs.199562.
- 553 8. Liesa M, Palacín M, Zorzano A. 2009. Mitochondrial Dynamics in Mammalian Health and
554 Disease. *Physiol Rev* 89:799–845.
- 555 9. Eisenreich W, Rudel T, Heesemann J, Goebel W. 2019. How Viral and Intracellular Bacterial
556 Pathogens Reprogram the Metabolism of Host Cells to Allow Their Intracellular Replication.
557 *Front Cell Infect Microbiol* 9:42.
- 558 10. Escoll P, Mondino S, Rolando M, Buchrieser C. 2016. Targeting of host organelles by
559 pathogenic bacteria: a sophisticated subversion strategy. *Nat Rev Microbiol* 14:5–19.
- 560 11. Lobet E, Letesson J-J, Arnould T. 2015. Mitochondria: A target for bacteria. *Biochem*
561 *Pharmacol* 94:173–185.

- 562 12. Spier A, Stavru F, Cossart P. 2019. Interaction between Intracellular Bacterial Pathogens and
563 Host Cell Mitochondria. *Microbiol Spectr* 7.
- 564 13. Khan M, Syed GH, Kim S-J, Siddiqui A. 2015. Mitochondrial dynamics and viral infections:
565 A close nexus. *Biochim Biophys Acta - Mol Cell Res* 1853:2822–2833.
- 566 14. Escoll P, Song O-R, Viana F, Steiner B, Lagache T, Olivo-Marin J-C, Impens F, Brodin P,
567 Hilbi H, Buchrieser C. 2017. *Legionella pneumophila* Modulates Mitochondrial Dynamics to
568 Trigger Metabolic Repurposing of Infected Macrophages. *Cell Host Microbe* 22:302-316.e7.
- 569 15. Chowdhury SR, Reimer A, Sharan M, Kozjak-Pavlovic V, Eulalio A, Prusty BK, Fraunholz
570 M, Karunakaran K, Rudel T. 2017. Chlamydia preserves the mitochondrial network necessary
571 for replication via microRNA-dependent inhibition of fission. *J Cell Biol* 216:1071–1089.
- 572 16. Stavru F, Bouillaud F, Sartori A, Ricquier D, Cossart P. 2011. *Listeria monocytogenes*
573 transiently alters mitochondrial dynamics during infection. *Proc Natl Acad Sci U S A*
574 108:3612–7.
- 575 17. Jain P, Luo Z-Q, Blanke SR. 2011. *Helicobacter pylori* vacuolating cytotoxin A (VacA)
576 engages the mitochondrial fission machinery to induce host cell death. *Proc Natl Acad Sci U S*
577 *A* 108:16032–7.
- 578 18. Stavru F, Palmer AE, Wang C, Youle RJ, Cossart P. 2013. Atypical mitochondrial fission
579 upon bacterial infection. *Proc Natl Acad Sci U S A* 110:16003–8.
- 580 19. Radoshevich L, Cossart P. 2018. *Listeria monocytogenes*: towards a complete picture of its
581 physiology and pathogenesis. *Nat Rev Microbiol* 16:32–46.
- 582 20. Schorr S, van der Laan M. 2017. Integrative functions of the mitochondrial contact site and
583 cristae organizing system. *Semin Cell Dev Biol*.
- 584 21. Kalia SK, Lee S, Smith PD, Liu L, Crocker SJ, Thorarinsdottir TE, Glover JR, Fon EA, Park

- 585 DS, Lozano AM. 2004. BAG5 inhibits parkin and enhances dopaminergic neuron
586 degeneration. *Neuron* 44:931–45.
- 587 22. Wang X, Guo J, Fei E, Mu Y, He S, Che X, Tan J, Xia K, Zhang Z, Wang G, Tang B. 2014.
588 BAG5 protects against mitochondrial oxidative damage through regulating PINK1
589 degradation. *PLoS One* 9:e86276.
- 590 23. Chen M, Chen Z, Wang Y, Tan Z, Zhu C, Li Y, Han Z, Chen L, Gao R, Liu L, Chen Q. 2016.
591 Mitophagy receptor FUNDC1 regulates mitochondrial dynamics and mitophagy. *Autophagy*
592 12:689–702.
- 593 24. Ma S, Zhang X, Zheng L, Li Z, Zhao X, Lai W, Shen H, Lv J, Yang G, Wang Q, Ji J. 2015.
594 Peroxiredoxin 6 Is a Crucial Factor in the Initial Step of Mitochondrial Clearance and Is
595 Upstream of the PINK1-Parkin Pathway. *Antioxid Redox Signal* 24:486–501.
- 596 25. Quintero OA, DiVito MM, Adikes RC, Kortan MB, Case LB, Lier AJ, Panaretos NS, Slater
597 SQ, Rengarajan M, Feliu M, Cheney RE. 2009. Human Myo19 is a novel myosin that
598 associates with mitochondria. *Curr Biol* 2009/11/26. 19:2008–2013.
- 599 26. Bohnert M, Zerbes RM, Davies KM, Mühleip AW, Rampelt H, Horvath SE, Boenke T, Kram
600 A, Perschil I, Veenhuis M, Kühlbrandt W, van der Klei IJ, Pfanner N, van der Laan M. 2015.
601 Central role of Mic10 in the mitochondrial contact site and cristae organizing system. *Cell*
602 *Metab* 21:747–55.
- 603 27. Barbot M, Jans DC, Schulz C, Denkert N, Kroppen B, Hoppert M, Jakobs S, Meinecke M.
604 2015. Mic10 oligomerizes to bend mitochondrial inner membranes at cristae junctions. *Cell*
605 *Metab* 21:756–63.
- 606 28. Li H, Ruan Y, Zhang K, Jian F, Hu C, Miao L, Gong L, Sun L, Zhang X, Chen S, Chen H, Liu
607 D, Song Z. 2016. Mic60/Mitofilin determines MICOS assembly essential for mitochondrial
608 dynamics and mtDNA nucleoid organization. *Cell Death Differ* 23:380–92.

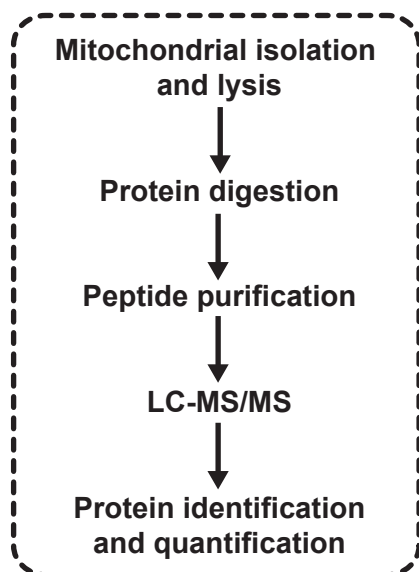
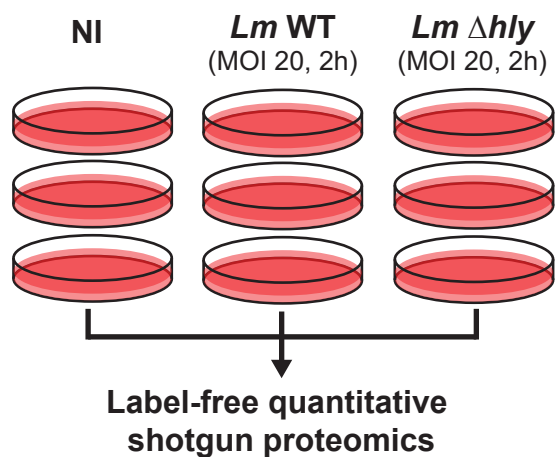
- 609 29. Callegari S, Müller T, Schulz C, Lenz C, Jans DC, Wissel M, Opazo F, Rizzoli SO, Jakobs S,
610 Urlaub H, Rehling P, Deckers M. 2019. A MICOS–TIM22 Association Promotes Carrier
611 Import into Human Mitochondria. *J Mol Biol.*
- 612 30. Kondadi AK, Anand R, Hänsch S, Urbach J, Zobel T, Wolf DM, Segawa M, Liesa M,
613 Shirihai OS, Weidtkamp-Peters S, Reichert AS. 2019. Cristae undergo continuous cycles of
614 fusion and fission in a MICOS-dependent manner. *bioRxiv* 654541.
- 615 31. Anand R, Strecker V, Urbach J, Wittig I, Reichert AS. 2016. Mic13 Is Essential for Formation
616 of Crista Junctions in Mammalian Cells. *PLoS One* 11:e0160258.
- 617 32. Koob S, Barrera M, Anand R, Reichert AS. 2015. The non-glycosylated isoform of MIC26 is
618 a constituent of the mammalian MICOS complex and promotes formation of crista junctions.
619 *Biochim Biophys Acta* 1853:1551–63.
- 620 33. Sirianni A, Krokowski S, Lobato-Márquez D, Buranyi S, Pfanzelter J, Galea D, Willis A,
621 Culley S, Henriques R, Larrouy-Maumus G, Hollinshead M, Sancho-Shimizu V, Way M,
622 Mostowy S, Lobato-Márquez D, Buranyi S, Pfanzelter J, Galea D, Willis A, Culley S,
623 Henriques R, Larrouy-Maumus G, Hollinshead M, Sancho-Shimizu V, Way M, Mostowy S.
624 2016. Mitochondria mediate septin cage assembly to promote autophagy of *Shigella*. *EMBO*
625 *Rep* 17:1029–43.
- 626 34. Lum M, Morona R. 2014. Dynamin-related protein Drp1 and mitochondria are important for
627 *Shigella flexneri* infection. *Int J Med Microbiol* 304:530–541.
- 628 35. Fine-Coulson K, Giguère S, Quinn FD, Reaves BJ. 2015. Infection of A549 human type II
629 epithelial cells with *Mycobacterium tuberculosis* induces changes in mitochondrial
630 morphology, distribution and mass that are dependent on the early secreted antigen, ESAT-6.
631 *Microbes Infect* 17:689–697.
- 632 36. Odendall C, Dixit E, Stavru F, Bierne H, Franz KM, Durbin AF, Boulant S, Gehrke L, Cossart

- 633 P, Kagan JC. 2014. Diverse intracellular pathogens activate type III interferon expression
634 from peroxisomes. *Nat Immunol* 2014/06/22. 15:717–726.
- 635 37. Jamwal S, Midha MK, Verma HN, Basu A, Rao KVS, Manivel V. 2013. Characterizing
636 virulence-specific perturbations in the mitochondrial function of macrophages infected with
637 *Mycobacterium tuberculosis*. *Sci Rep* 3:1328.
- 638 38. Stauch KL, Purnell PR, Fox HS. 2014. Quantitative proteomics of synaptic and nonsynaptic
639 mitochondria: insights for synaptic mitochondrial vulnerability. *J Proteome Res* 13:2620–36.
- 640 39. Gómez-Serrano M, Camafeita E, López JA, Rubio MA, Bretón I, García-Consuegra I, García-
641 Santos E, Lago J, Sánchez-Pernaute A, Torres A, Vázquez J, Peral B. 2017. Differential
642 proteomic and oxidative profiles unveil dysfunctional protein import to adipocyte
643 mitochondria in obesity-associated aging and diabetes. *Redox Biol* 11:415–428.
- 644 40. Alkhaja AK, Jans DC, Nikolov M, Vukotic M, Lytovchenko O, Ludewig F, Schliebs W,
645 Riedel D, Urlaub H, Jakobs S, Deckers M. 2012. MINOS1 is a conserved component of
646 mitofilin complexes and required for mitochondrial function and cristae organization. *Mol*
647 *Biol Cell* 23:247–57.
- 648 41. Rampelt H, Bohnert M, Zerbes RM, Horvath SE, Warscheid B, Pfanner N, van der Laan M.
649 2017. Mic10, a Core Subunit of the Mitochondrial Contact Site and Cristae Organizing
650 System, Interacts with the Dimeric F1Fo-ATP Synthase. *J Mol Biol* 429:1162–1170.
- 651 42. Eydt K, Davies KM, Behrendt C, Wittig I, Reichert AS. 2017. Cristae architecture is
652 determined by an interplay of the MICOS complex and the F1FO ATP synthase via Mic27
653 and Mic10. *Microb cell (Graz, Austria)* 4:259–272.
- 654 43. Harner M, Körner C, Walther D, Mokranjac D, Kaesmacher J, Welsch U, Griffith J, Mann M,
655 Reggiori F, Neupert W. 2011. The mitochondrial contact site complex, a determinant of
656 mitochondrial architecture. *EMBO J* 30:4356–4370.

- 657 44. Tang J, Zhang K, Dong J, Yan C, Hu C, Ji H, Chen L, Chen S, Zhao H, Song Z. 2019. Sam50-
658 Mic19-Mic60 axis determines mitochondrial cristae architecture by mediating mitochondrial
659 outer and inner membrane contact. *Cell Death Differ* 1.
- 660 45. Stoldt S, Stephan T, Jans DC, Brüser C, Lange F, Keller-Findeisen J, Riedel D, Hell SW,
661 Jakobs S. 2019. Mic60 exhibits a coordinated clustered distribution along and across yeast and
662 mammalian mitochondria. *Proc Natl Acad Sci* 201820364.
- 663 46. Wiedemann N, Pfanner N. 2017. Mitochondrial Machineries for Protein Import and
664 Assembly. *Annu Rev Biochem* 86:685–714.
- 665 47. Ueda E, Tamura Y, Sakaue H, Kawano S, Kakuta C, Matsumoto S, Endo T. 2019. Myristoyl
666 group-aided protein import into the mitochondrial intermembrane space. *Sci Rep* 9:1185.
- 667 48. Quirós PM, Langer T, López-Otín C. 2015. New roles for mitochondrial proteases in health,
668 ageing and disease. *Nat Rev Mol Cell Biol* 16:345–59.
- 669 49. Dramsi S, Cossart P. 2003. Listeriolysin O-mediated calcium influx potentiates entry of
670 *Listeria monocytogenes* into the human Hep-2 epithelial cell line. *Infect Immun* 71:3614–
671 3618.
- 672 50. Vadia S, Seveau S. 2014. Fluxes of Ca²⁺ and K⁺ are required for the listeriolysin O-
673 dependent internalization pathway of *Listeria monocytogenes*. *Infect Immun* 82:1084–1091.
- 674 51. Mallilankaraman K, Doonan P, Cárdenas C, Chandramoorthy HC, Müller M, Miller R,
675 Hoffman NE, Gandhirajan RK, Molgó J, Birnbaum MJ, Rothberg BS, Mak D-OD, Foskett
676 JK, Madesh M. 2012. MICU1 Is an Essential Gatekeeper for MCU-Mediated Mitochondrial
677 Ca²⁺ Uptake that Regulates Cell Survival. *Cell* 151:630–644.
- 678 52. Palty R, Silverman WF, Hershinkel M, Caporale T, Sensi SL, Parnis J, Nolte C, Fishman D,
679 Shoshan-Barmatz V, Herrmann S, Khananshvili D, Sekler I. 2010. NCLX is an essential
680 component of mitochondrial Na⁺/Ca²⁺ exchange. *Proc Natl Acad Sci U S A* 107:436–41.

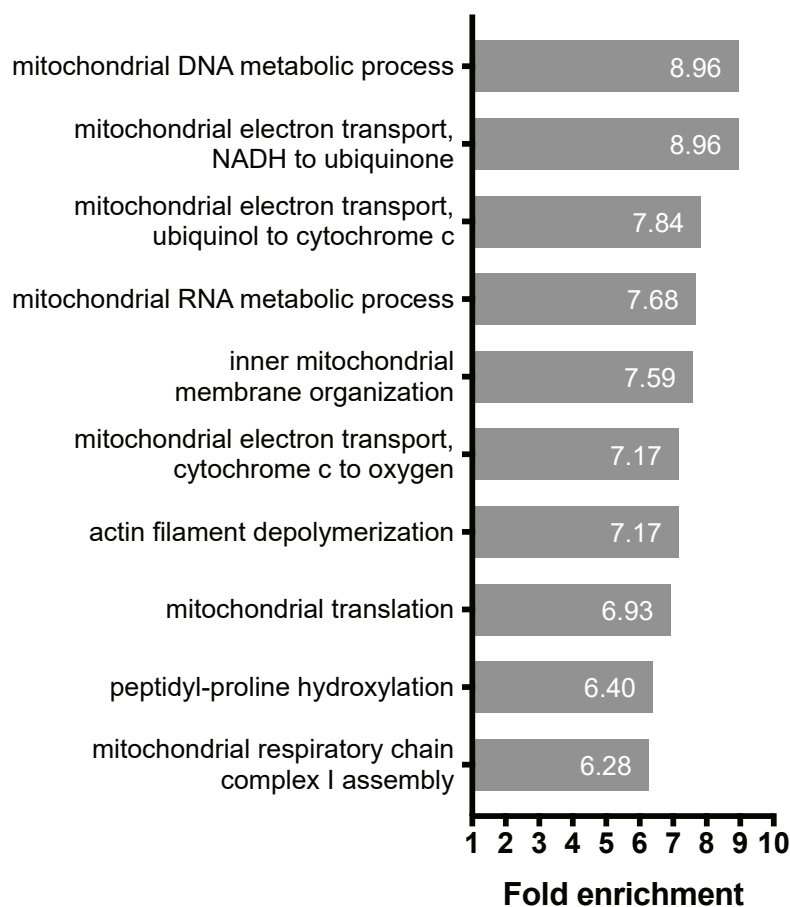
- 681 53. Kostic M, Ludtmann MHR, Bading H, Hershinkel M, Steer E, Chu CT, Abramov AY, Sekler
682 I. 2015. PKA Phosphorylation of NCLX Reverses Mitochondrial Calcium Overload and
683 Depolarization, Promoting Survival of PINK1-Deficient Dopaminergic Neurons. *Cell Rep*
684 13:376–386.
- 685 54. Hom JR, Gewandter JS, Michael L, Sheu S-S, Yoon Y. 2007. Thapsigargin induces biphasic
686 fragmentation of mitochondria through calcium-mediated mitochondrial fission and apoptosis.
687 *J Cell Physiol* 212:498–508.
- 688 55. Valente AJ, Maddalena LA, Robb EL, Moradi F, Stuart JA. 2017. A simple ImageJ macro
689 tool for analyzing mitochondrial network morphology in mammalian cell culture. *Acta*
690 *Histochem* 119:315–326.
- 691 56. Perez-Riverol Y, Csordas A, Bai J, Bernal-Llinares M, Hewapathirana S, Kundu DJ, Inuganti
692 A, Griss J, Mayer G, Eisenacher M, Pérez E, Uszkoreit J, Pfeuffer J, Sachsenberg T, Yilmaz
693 Ş, Tiwary S, Cox J, Audain E, Walzer M, Jarnuczak AF, Ternent T, Brazma A, Vizcaíno JA.
694 2019. The PRIDE database and related tools and resources in 2019: improving support for
695 quantification data. *Nucleic Acids Res* 47:D442–D450.
- 696
- 697

A



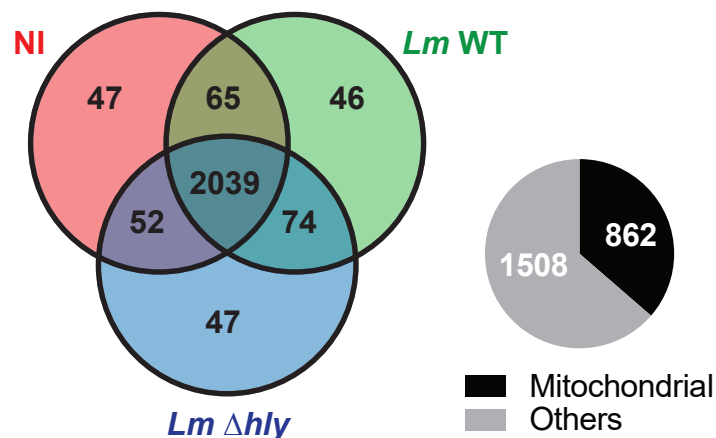
C

Top 10 enriched GO Biological Processes



B

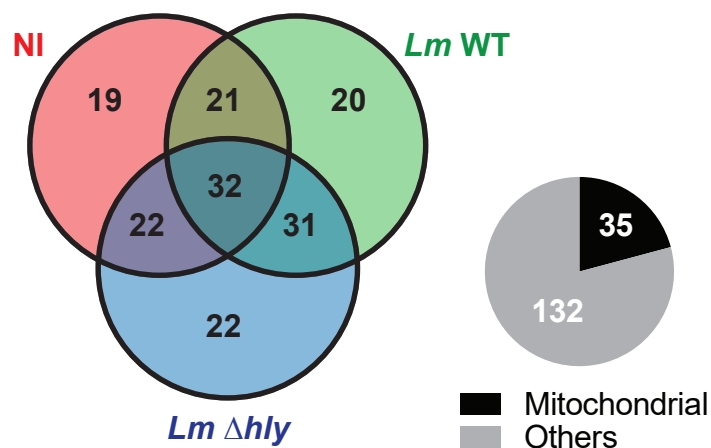
Total identified proteins: 2370



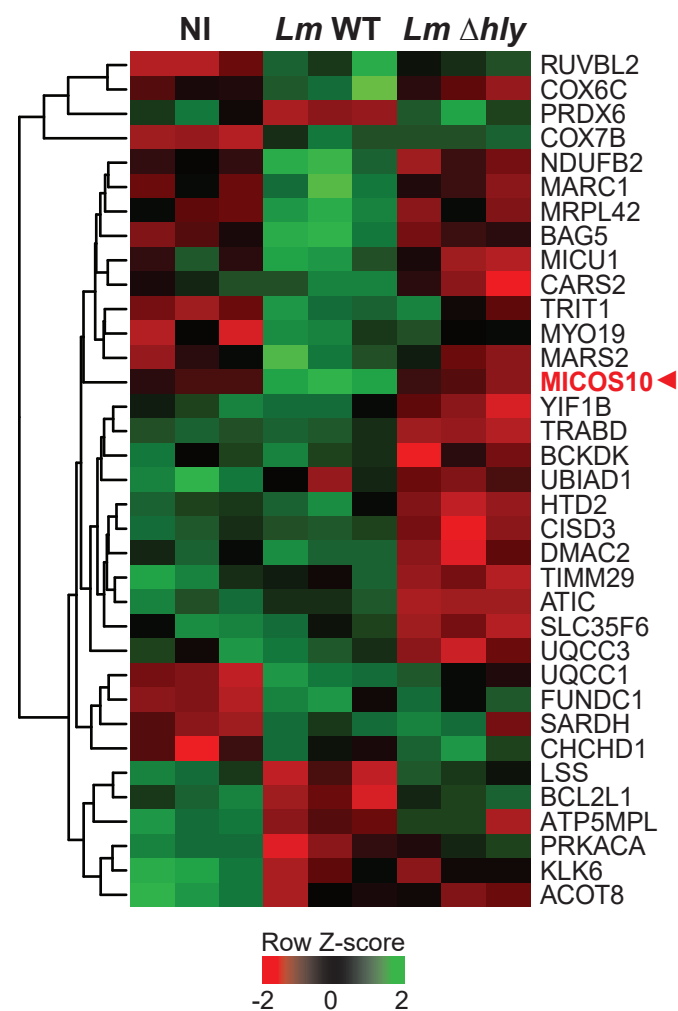
D

Differentially abundant proteins: 167

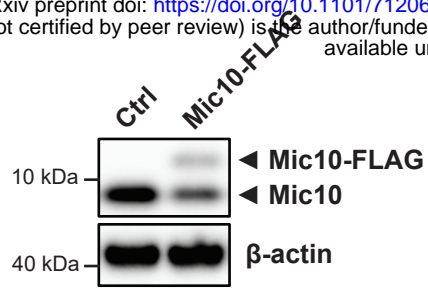
(fold change > 2; FDR = 0.05)



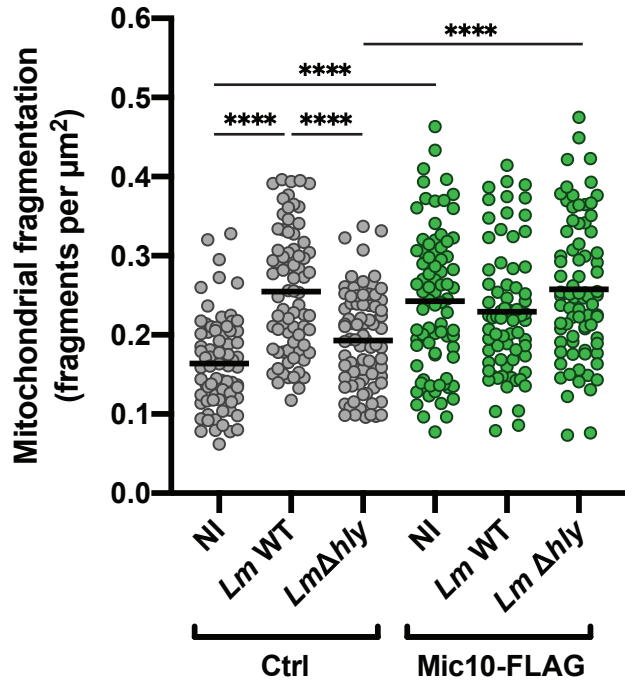
E



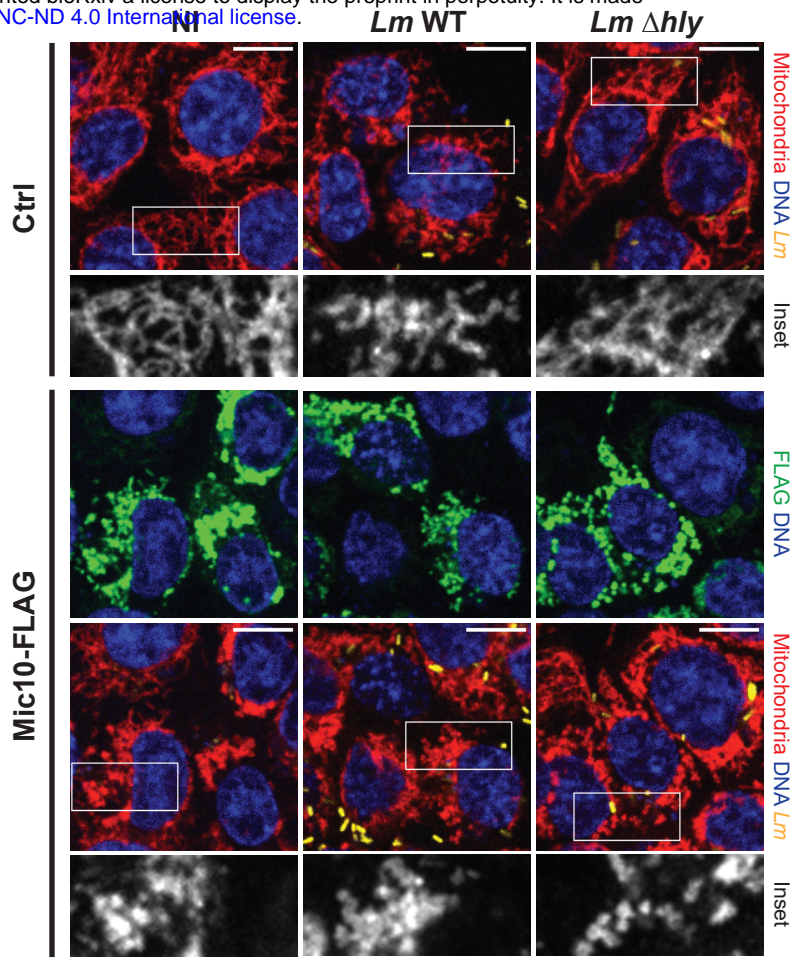
A



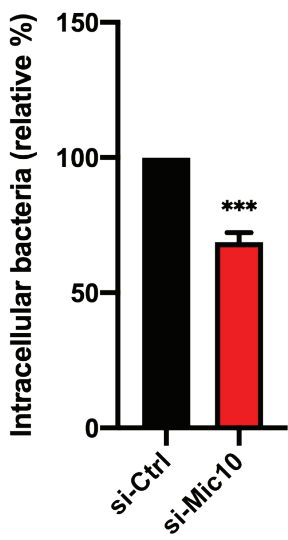
C



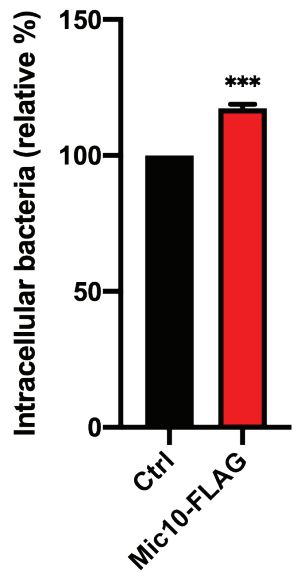
B



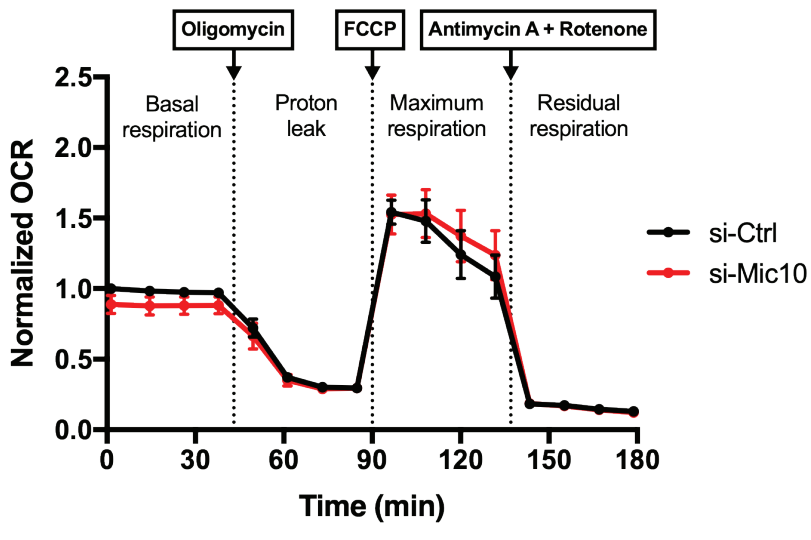
A



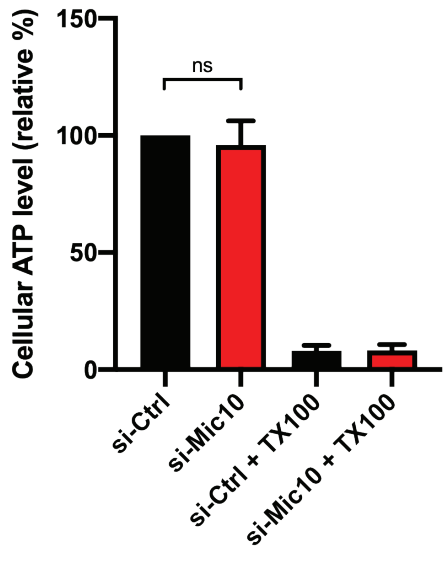
B



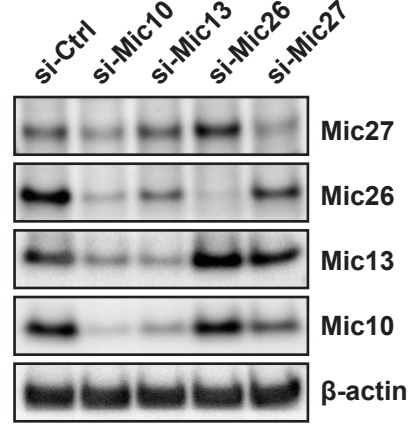
C



D



E



F

